Micelles, Dispersions, and Liquid Crystals in the Catanionic Mixture Bile Salt−Double-Chained Surfactant. The Bile Salt-Rich Area

Eduardo F. Marques,*[,†,‡] Oren Regev,[§] Håkan Edlund,[||] and Ali Khan[†]

Physical Chemistry 1, Center for Chemistry and Chemical Engineering, P.O. Box 124, Lund University, Lund SE-221 00, Sweden, Department of Chemical Engineering, Ben-Gurion University of the Negev, P.O. Box 653, 84105 Beer-Sheva, Israel, Departamento de Química, Universidade de Coimbra, 3049 Coimbra, Portugal, and Department of Chemistry and Process Technology, Chemistry, Mid Sweden University, SE-851 70 Sundsvall, Sweden

Received February 15, 2000. In Final Form: August 1, 2000

The phase behavior and phase structure for the catanionic pair sodium taurodeoxycholate−didodecyldimethylammonium bromide (DDAB) are investigated, at 25 °C. A combination of techniques is used including light and electron microscopy, small-angle X-ray scattering, and pulsed field gradient NMR self-diffusion. The bile salt micellar solution incorporates large amounts of the double-chained amphiphile, with the solution region extending to equimolarity. On the contrary, the hexagonal liquid-crystalline phase is destabilized by the addition of small amounts of DDAB. At equimolarity, coacervation instead of precipitation is observed, with formation of a viscous isotropic solution and a very dilute one. In the water-rich part of the phase diagram, a peculiar type of phase separation occurs, involving the formation of very fine bluish dispersions and a region of coexistence of two dispersions (*double dispersion* region). Microscopy and self-diffusion data for the solution region indicate limited growth of the mixed micelles. Large domains in which the micellar structure appears to be maintained are imaged in the bluish dispersions by electron microscopy. No other type of aggregate such as vesicles or precipitates is observed in the dilute bile salt-rich area of this mixture.

1. Introduction

The bile acid salts are surfactants of vital biological importance. They play an active role in the emulsification of fats in the gut and aid in the excretion process of lecithin and cholesterol.[1−3] The surface and aggregation properties of aqueous solutions of bile salts have been scrutinized over decades.[4−13] It is known that the molecules form micelles of small aggregation numbers and that these aggregates grow with concentration.[8,9,14−16] Between the isotropic solution and the hydrated crystals, a narrow region of hexagonal liquid crystal formation has been recently found for various types of bile salts.[17,18] The uncommon properties of these surfactants are directly linked to their molecular structure, in particular the absence of flexible alkyl chains and the dual polar/nonpolar character of the hydroxylated steroid ring. The aggregation process is essentially due to hydrophobic "back-to-back" interactions, but intermolecular hydrogen bonding seems also to play a role.[10,16,19]

Owing to the natural occurrence of bile salts in complex mixtures with other compounds, phase behavior investigations have naturally extended to ternary and quaternary systems where bile salt is mixed with phospholipids,[20−27] monoglycerides,[28] or several common synthetic surfactants.[29−32] Various types of micellar and vesicular aggregates have been directly imaged in human bile.[33] In

* To whom correspondence may be addressed. E-mail: eduardo.marques@fkem1.lu.se or emarques@ci.uc.pt.
† Lund University.
‡ Universidade de Coimbra.
§ Ben-Gurion University of the Negev.
|| Mid Sweden University.

(1) Carey, M. C.; Small, D. M. *Am. J. Med.* **1970**, *49*, 590.
(2) Small, D. M. *The Bile Acids*; Nair, P. P., Kritchevsky, D., Eds.; Plenum Press: New York, 1971.
(3) Borgström, B. *Int. Rev. Physiol.* **1977**, *12*, 305.
(4) Ekwall, P. *J. Colloid Sci.* **1954**, *8*, 66.
(5) Blow, D. M.; Rich. A. *J. Am. Chem. Soc.* **1960**, *82*, 3566.
(6) Fontell, K. *Kolloid-Z. Z. Polym.* **1971**, *244*, 246.
(7) Carey, M. C.; Small, D. M. *Arch. Intern. Med.* **1972**, *130*, 506.
(8) Mysels, K. J. *Hepatology* **1984**, *4*, 80S.
(9) Mazer, N. A.; Carey, M. C.; Kwasnick, R. F.; Benedek, G. B. *Biochemistry* **1979**, *18*, 3064.
(10) Murata, Y.; Sugihara, G.; Fukushima, K.; Tanaka, M.; Matsushita, K. *J. Phys. Chem.* **1982**, *86*, 4690.
(11) Kratohvil, J. P.; Hsu, W. P.; Kwok, D. I. *Langmuir* **1986**, *2*, 256.
(12) Giglio, E.; Loreti, S.; Pavel, N. V. *J. Phys. Chem.* **1988**, *92*, 2858.
(13) Briganti, G.; D'Archivio, A. A.; Galantini, L.; Giglio, E. *Langmuir* **1996**, *12*, 1180.
(14) Lindman, B.; Kamenka, N.; Brun, B. *J. Colloid Interface Sci.* **1976**, *56*, 238.
(15) Kratohvil, J. P. *Adv. Colloid Interface Sci.* **1986**, *26*, 131.
(16) Li, G.; McGown, L. B. *J. Phys. Chem.* **1994**, *98*, 13711.
(17) Edlund, H.; Khan, A.; La Mesa, C. *Langmuir* **1998**, *14*, 3691.
(18) Marques, E. F.; Edlund, H.; La Mesa, C.; Khan, A. *Langmuir* **2000**, *16*, 5178−5186.
(19) Ju, C.; Bohne, C. *J. Phys. Chem.* **1996**, *100*, 3847.
(20) Ulmius, J.; Lindblom, G.; Wennerström, H.; Johansson, L. B.-Å.; Fontell, K.; Söderman, O.; Arvidson, G. *Biochemistry* **1982**, *21*, 1553.
(21) Thurmond, R. L.; Lindblom, G.; Brown, M. F. *Biophys. J.* **1991**, *60*, 728.
(22) Walter, A.; Vinson, P. K.; Kaplon, A.; Talmon, Y. *Biophys J.* **1991**, *60*, 1315.
(23) Edwards, K.; Almgren, M. *Langmuir* **1992**, *8*, 824.
(24) Pedersen, J. S.; Egelhaaf, S. U.; Schurtenberger, P. *J. Phys. Chem.* **1995**, *99*, 1299.
(25) Li, C.-Y.; Wiedmann, T. S. *J. Phys. Chem.* **1996**, *100*, 18464.
(26) Luk, A. S.; Kaler, E. W.; Lee, S. P. *Biochemistry* **1997**, *36*, 5633.
(27) Cohen, D. E.; Thurston, G. M.; Chamberlin, R. A.; Benedek, G. B.; Carey, M. C. *Biochemistry* **1998**, *37*, 14798.
(28) Svärd, M.; Schurtenberger, P.; Fontell, K.; Jönsson, B.; Lindman, B. *J. Phys. Chem.* **1988**, *92*, 2261.
(29) Barry, B. W.; Gray, G. M. T. *J. Colloid Interface Sci.* **1975**, *52*, 327.
(30) La Mesa, C.; Khan, A.; Fontell, K.; Lindman, B. *J. Colloid Interface Sci.* **1985**, *103*, 373−391.
(31) Wu, K.; McGown, L. B. *J. Phys. Chem.* **1994**, *98*, 1185.
(32) Swanson-Vethamuthu, M.; Almgren, M.; Bergenståhl, B.; Mukhtar, E. *J. Colloid Interface Sci.* **1996**, *178*, 538.
(33) Kaplun, A.; Talmon, Y.; Konikoff, F. M.; Rubin, M.; Eitan, A.; Tadmor, M.; Lichtenberg, D. *FEBS Lett.* **1994**, *340*, 78.

10.1021/la0002278 CCC: $19.00
Published on Web 10/07/2000

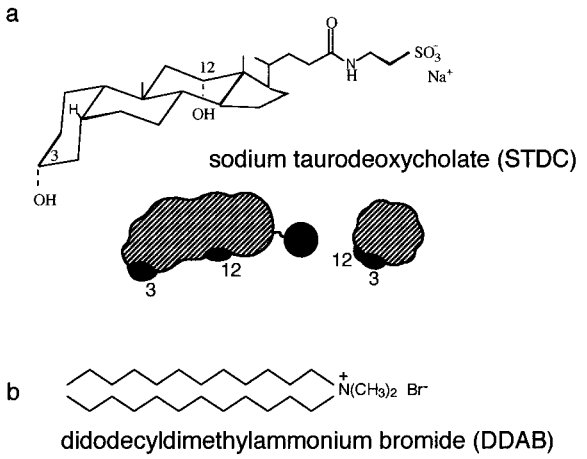

Figure 1. Molecular structure of the catanionic pair: (a) the bile salt sodium taurodeoxycholate (3α,12α-dihydroxy-5β-taurocholan-24-oic acid salt), STDC, together with a longitudinal and transverse view of the molecule; (b) the double-chained surfactant didodecyldimethylammonium bromide (DDAB).

the sodium cholate−lecithin−water system,[20] for example, extensive micellar solution and lamellar liquid-crystalline phases are formed, as well as hexagonal and cubic phases, indicating strong amphiphilic association. Mixed systems comprising sodium deoxycholate and anionic surfactants, such as sodium bis(2-diethylhexyl)sulfosuccinate (AOT), sodium didodecyl sulfate (SDS), Triton X-100, and hexadecyltrimethylammonium bromide (CTAB)[32,34] have also been studied. In the *catanionic system* sodium deoxycholate−CTAB, separation into two coexisting liquids (*coacervation*) is seen at equimolar ratio, instead of precipitation.[32] Borne out from the latter studies is the great versatility of bile salts to associate with different surfactants, either oppositely or similarly charged.

In the current work, the associative behavior between a bile salt and a double-chained surfactant of opposite charge is addressed. This type of *catanionic mixture* has not been investigated previously, and it is anticipated to yield interesting features, since the aggregation properties of the two amphiphiles in water are very different. Sodium taurodeoxycholate (STDC), one of the most widespread bile acids, and the double-chained surfactant didodecyldimethylammonium bromide (DDAB) are the catanionic pair to be investigated at room temperature (Figure 1). Only the bile salt-rich area is reported here, while the DDAB-rich one will be addressed in a separate work. The interplay between the electrostatic interactions and different geometric packing properties of the two amphiphiles will dictate the phase behavior features in the STDC−DDAB mixture. The DDAB surfactant, with a packing parameter of about 0.8, has a tendency to form lamellar liquid crystals[35−37] and, at high dilution, vesicle dispersions,[38−40] while the bile salt molecule packs into micellar-like aggregates. The net outcome of electrostatic/packing interactions at both macroscopic level (phase behavior) and microscopic level (aggregate structure) remains to be seen.

The strong associative phase behavior in catanionic systems usually leads to the formation of crystalline precipitates around equimolarity and several "novel" liquid-crystalline phases.[41,42] This type of behavior is seen inter alia for the systems DDAB−SDS[37] and DDAB−AOT.[43] At low concentrations, with slight excess of one of the ionic amphiphiles, mixed micelles denoting growth (to rodlike or disklike micelles) and stable, spontaneous vesicles are often formed.[40,44−46] In this context, several particular issues are addressed here: (i) type of associative phase separation (precipitation, coacervation, or liquid crystal formation); (ii) nature of micellar growth; (iii) possible formation of vesicles and "novel" liquid-crystalline phases.

2. Experimental Section

2.1. Materials and Sample Preparation. Sodium taurodeoxycholate (STDC), 0.5 mol of H_2O/mol, more than 97% in purity, was purchased from Sigma and used without further purification. Didodecyldimethylammonium bromide (DDAB) of high purity was obtained from Tokyo Kasei. D_2O supplied by Dr. Basel, Switzerland, was used in all samples for self-diffusion NMR. The molecular structure of STDC and DDAB is shown in parts a and b of Figure 1, respectively. The two hydroxyl groups (αC-3 and αC-12) in STDC point to the same side of the steroid ring, giving it a polar and a nonpolar side. The relative spacial position of the two carbon atoms is easily visualized in the shaded space filling models in Figure 1a. The samples were prepared by weighing directly the two surfactant solids into glass vials and thoroughly mixing them in water end-over-end for at least 24 h.

2.2. Phase Behavior and Structure Determination. *Phase Diagram.* The phase diagram in Figure 2 results from the analysis of ca. 150 samples in the course of at least 6 months. The samples were inspected by the naked eye and between crossed polaroids in order to check for birefringence. Phase assignment is further done on the basis of combined polarizing microscopy, cryogenic transmission electron microscopy (cryo-TEM), self-diffusion NMR, and small angle X-ray scattering (SAXS). The uncertainty of boundaries in the phase diagrams is ca. ±2 wt % in Figure 2 and less than ±0.5 wt % in Figure 4.

Light Microscopy. An Axioplan Universal polarizing light microscope (Carl Zeiss) was used, equipped with differential interference contrast (DIC) lenses and a high-sensitive videocamera system, with image processor Argus-20 (Hamamatsu Photonics, Japan).

Small-Angle X-ray Scattering (SAXS). The measurements were carried out in a Kratky camera system equipped with a position-sensitive detector with 1024 channels of width 53 μm. The Cu Kα radiation of wavelength 1.542 Å was used, and the sample-to-detector distance was 277 mm. The samples were prepared in a paste holder between thin mica windows. The temperature was regulated by a Peltier element and the camera volume kept under vacuum to minimize air scattering.

Cryogenic Transmission Electron Microscopy (cryo-TEM). The cryo-TEM method[47,48] was used for direct imaging of dilute solutions and bluish dispersions. When artifact-free films are

(34) La Mesa, C.; Khan, A.; Fontell, K.; Lindman, B. *J. Colloid Interface Sci.* **1985**, *103*, 373.
(35) Fontell, K.; Ceglie, A.; Lindman, B.; Ninham, B. *Acta Chem. Scand.* **1986**, *A40*, 247.
(36) Zemb, T.; Gazeau, D.; Dubois, M.; Gulik-Krzywicki, T. *Europhys. Lett.* **1993**, *21*, 759.
(37) Marques, E.; Khan, A.; Miguel, M. G.; Lindman, B. *J. Phys. Chem.* **1993**, *97*, 4729.
(38) Miller, D. D.; Bellare, J. R.; Evans, D. F.; Talmon, Y.; Ninham, B. W. *J. Phys. Chem.* **1987**, *91*, 674.
(39) Dubois, M.; Zemb, T. *Langmuir* **1991**, *7*, 1352.
(40) Marques, E. F.; Regev, O.; Khan, A.; Miguel, M. G.; Lindman, B. *J. Phys. Chem.* **1999**, *103*, 8353.
(41) Jokela, P.; Jönsson, B.; Khan, A. *J. Phys. Chem.* **1987**, *91*, 3291−3298.
(42) Khan, A.; Marques, E. Catanionic Surfactants. In *Specialists Surfactants*; Robb, I. D., Ed.; Blackie Academic and Professional, an imprint of Chapman & Hall: London, 1997; pp 37−76.
(43) Caria, A.; Khan, A. *Langmuir* **1996**, *12*, 6282.
(44) Kaler, E. W.; Murthy, A. K.; Rodriguez, B. E.; Zasdzinski, J. A. N. *Science* **1989**, *245*, 1371.
(45) Kaler, E. W.; Herrington, K. L.; Murthy, A. K.; Zasadzinski, J. A. *J. Phys. Chem.* **1992**, *96*, 6698−6707.
(46) Marques, E. F.; Regev, O.; Khan, A.; Miguel, M. G.; Lindman, B. *J. Phys. Chem. B* **1998**, *102*, 6746.
(47) Bellare, J. R.; Davis, H. T.; Scriven, L. E.; Talmon, Y. *J. Electron Microsc. Technol.* **1988**, *10*, 87.
(48) Vinson, P. K. "Cryo-TEM, carbon-coated holey polymer film"; The 45th Annual Meeting of the Electron Microscopy Society of America, San Francisco, CA, 1987.

prepared, this method is powerful in the structural investigation of surfactant systems.[49] Vitrified samples were prepared and imaged according to the procedure described in previous works.[40,46]

Pulsed-Field Gradient (PFG) NMR Self-Diffusion. The PFG technique for measuring self-diffusion coefficients is very useful for structural and dynamic studies in surfactant systems.[50,51] The method is based on a combination of radio frequency (rf) pulses and magnetic field gradient pulses, as described in detail in specialist reviews.[52,53] In this work, measurements were done in a Bruker DMX200 spectrometer at 25 °C, with a probe providing a maximum gradient of 9 T/m. The water and the surfactant self-diffusion were measured by means of the *basic Hahn echo* and the *stimulated echo* sequence, respectively, as described in detail in previous work.[18,46]

3. Results and Discussion

3.1. Overview of Phase Behavior. The phase behavior for the catanionic system STDC−DDAB−water, in the bile salt-rich area, at 25 °C is depicted in the triangular phase diagram in Figure 2. The compositions are given in wt % for the three chemical species and represented by a point in the triangle. Throughout the discussion, the surfactant mixing ratio is given by the DDAB molar fraction, $X_{DDAB} = n_{DDAB}/(n_{STDC} + n_{DDAB})$, where n_i is the number of moles of component i in the sample. It should be kept in mind that catanionic mixtures are, strictly speaking, four-component systems,[54,55] but often, on the basis of experimental data, their phase behavior can be conveniently depicted by ternary phase diagrams.[37,43,56]

At room temperature, the bile salt STDC is soluble in water up to about 26 wt %. The isotropic solution contains at the critical micelle concentration (cmc) micellar aggregates of small aggregation number, and as the amphiphile concentration rises, the aggregates grow into larger micelles. In the range 37−60 wt %, an anisotropic liquid-crystalline phase is formed, as recently shown by Edlund et al.[17] It is now known, contrary to previous notions, that several bile salts form a common type of anisotropic liquid-crystalline phase.[18] DDAB, on the other hand, is a highly insoluble surfactant, forming at room temperature two lamellar liquid-crystalline phases, a concentrated one and a dilute one. Below 3 wt % in water, the amphiphile forms a lamellar dispersion, where different types of vesicular structures are identified (uni-, bi-, and multilamellar vesicles).[38−40,57]

As can be seen in Figure 2, the addition of the bilayer-forming surfactant to the bile salt solution results in several interesting effects. Up to about 20 wt % STDC, the maximum amount of DDAB solubilized is roughly constant at $X_{DDAB} = 0.3$. The solutions are clear and increasingly viscous. For more than 20 wt % STDC, the solution region forms a long "neck" which extends up to equimolar composition. This observation implies that increasing amounts of DDAB are taken up by the solution phase as the STDC concentration rises. The equimolar solution phase, which has a narrow stability range (36−40 wt % STDC and 28−32 wt % DDAB), is also clear and extremely viscous. It incorporates only a small excess of DDAB prior to phase separation (Figure 2). Along the equimolar line, the concentrated L_1 phase is in equilibrium with a low-viscosity clear liquid (L in Figure 2), which is almost "pure" water, i.e., a *coacervation* region is formed. Between the L_1 phase and the two-phase $L_1 + L$ region (where both solutions are *clear*), there is another liquid−liquid coexistence region in which at least one of the liquids is *bluish* and weakly translucent (L + bluish disp region in Figure 2). As discussed further, the macroscopic appearance of the two coexisting liquids changes drastically as X_{DDAB} increases toward equimolarity (Figure 5). Up to about 20 wt % STDC and $X_{DDAB} \approx 0.30-0.35$, the bluish dispersion shows macroscopically homogeneous, forming a narrow strip in the phase diagram (Figure 2). The liquid-crystalline phase (lc region in Figure 2) incorporates smaller amounts of DDAB than the solution phase, with no more than 11 mol % DDAB (at 45 wt % STDC) being solubilized. As the STDC concentration increases beyond 45 wt %, increasingly lower amounts of DDAB are taken up by the lc phase. Beyond the solubilty limits, a two-phase region lc + L_1 and a three-phase region L_1 + lc + hydrated crystals are formed.

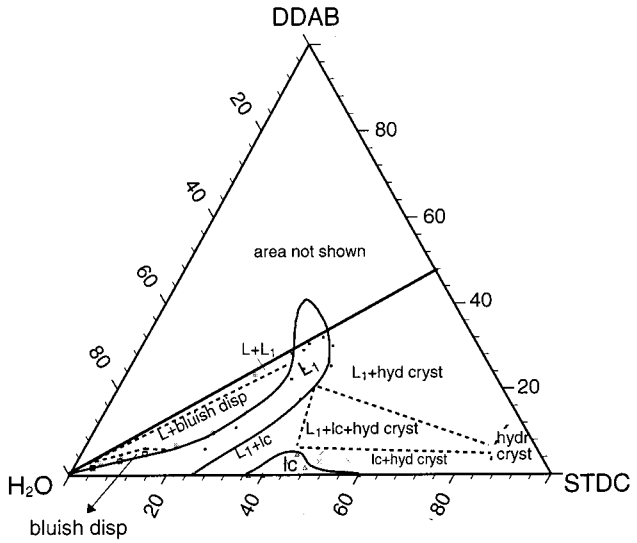

Figure 2. Phase behavior for the system STDC−DDAB−water at 25 °C, in the bile salt-rich area. Notations are as follows: L_1, isotropic solution; L, very dilute isotropic solution; bluish disp, bluish dispersion; lc, liquid crystal; cryst, hydrated crystals. The straight line drawn is the equimolarity line.

3.2. The Liquid-Crystalline Phase. Both SAXS measurements and optical textures show that the lc phase in the STDC−DDAB−water system is of the hexagonal type. In Figure 3a, a series of Bragg reflections in the order 1:1.73:1.98:2.66 are detected for a representative sample at 43.2 wt % STDC/3.02 wt % DDAB. The q values are in good agreement with the expected $1:\sqrt{3}:\sqrt{4}:\sqrt{7}$ sequence for a hexagonal liquid-crystalline phase. To be noticed is the low intensity of the correlation peaks and the fact that the first (01) reflection is of comparable intensity to the successive (11), (21), and (22) peaks. For this sample, a d-spacing of 4 nm and a nearest-neighbor distance between cylinders of 4.6 nm were obtained. We note that these values are compatible with a hexagonal phase of the reverse type (even if its structure may not follow the conventional type), as previously proposed for the binary bile salt−water lc phase.[17,18] In the polarizing microscope, a nongeometric, striated pattern, typical of a hexagonal phase, is observed (Figure 3b). ^{2}H NMR spectra

(49) Talmon, Y. *Ber. Bunsen-Ges. Phys. Chem.* **1996**, *3*, 364.
(50) Lindman, B.; Söderman, O.; Wennerström, H. NMR studies of surfactant systems. In *Surfactant Solutions, New Methods of Investigation*; Zana, R., Ed.; Marcel Dekker: New York, 1987.
(51) Söderman, O.; Stilbs, P. *Prog. Nucl. Magn. Reson. Spectrosc.* **1994**, *26*, 445.
(52) Stilbs, P. *Prog. Nucl. Magn. Reson. Spectrosc.* **1987**, *19*, 1.
(53) Price, W. S. *Concepts Magn. Res.* **1997**, *9*, 299.
(54) Jokela, P.; Jönsson, B.; Wennerström, H. *Prog. Colloid Polym. Sci.* **1985**, *70*, 17−22.
(55) Thalberg, K.; Lindman, B. Polyelectrolyte-ionic surfactant systems. In *Surfactants in Solution*; Mittal, K., Shah, O. O., Eds.; Plenum Press: New York, 1991.
(56) Regev, O.; Khan, A. *J. Colloid Interface Sci.* **1996**, *182*, 95.
(57) Regev, O.; Khan, A. *Prog. Colloid Polym. Sci.* **1994**, *97*, 298.

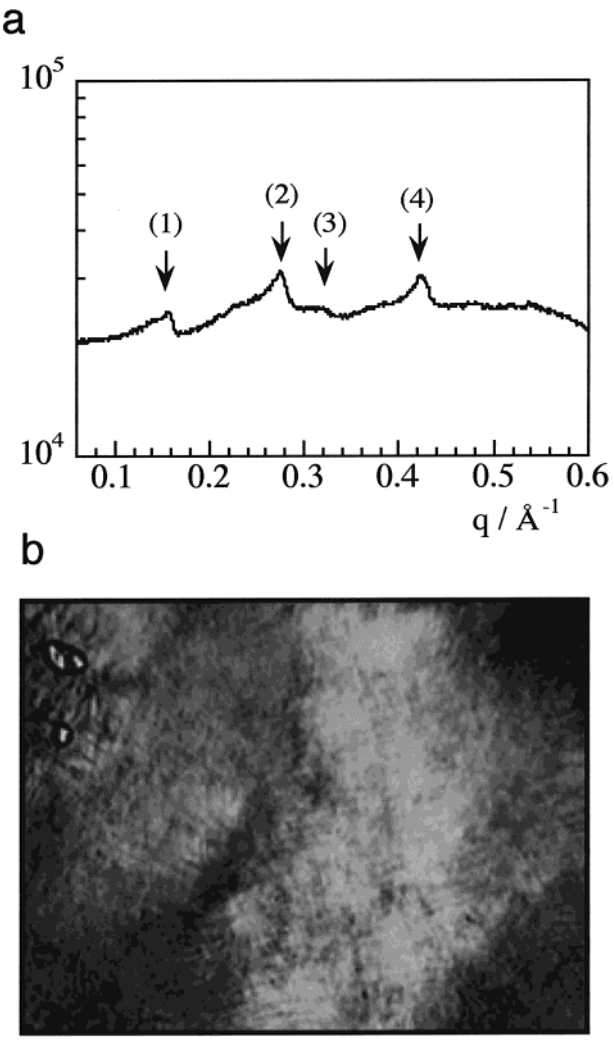

Figure 3. Structural determination of the liquid crystal (at 41 wt % STDC, 4 wt % DDAB): (a) slit-smeared SAXS pattern, where the numbers indicate the *n*th order correlation peak ascribed to a hexagonal lattice; (b) nongeometric striated texture at the polarizing microscope, typical of a hexagonal phase.

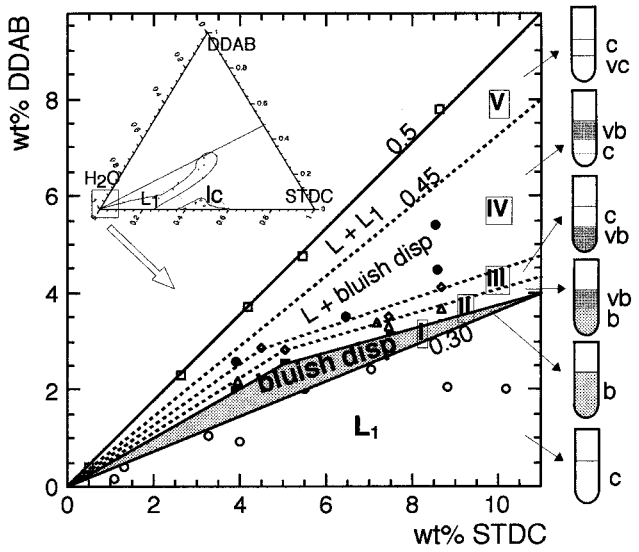

Figure 4. Detailed phase behavior for the system STDC−DDAB−water at 25 °C in the water-rich corner. The insert shows the complete phase diagram. In the right-hand side the macroscopic appearance of the samples in the test tube is depicted. Legend: c, colorless; b, bluish (low-viscosity); vb, viscous bluish (high-viscosity); vc, viscous clear.

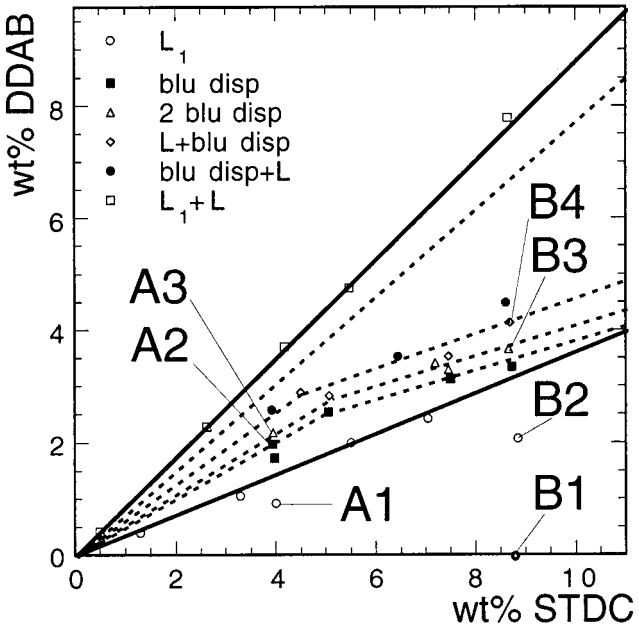

Figure 5. Location of the samples imaged by cryo-TEM and light microscopy in the dilute phase diagram.

recorded for several samples within the lc region varied between an incipient quadrupolar splitting and a broad singlet, depending on sample composition, similar to data reported for the bile salt−water systems.[18]

3.3. Structural Investigation of Solutions and Bluish Dispersions. A. Macroscopic View of Phase Separation. The phase behavior in the water-rich area of the catanionic mixture is depicted in Figure 4, with a detailed view of the area between the L_1 phase and the equimolar line. For easier visualization, a phase map is shown where the sample composition is plot as DDAB wt % vs STDC wt %. Some peculiar aspects of phase separation are observed. Five different areas are identified between the L_1 phase (at roughly constant $X_{DDAB} = 0.30$) and the equimolarity line (at $X_{DDAB} = 0.50$). Initially, a bluish nonbirefringent liquid is seen (region I). This region is followed by a liquid−liquid coexistence region (region II): the upper liquid is bluish, turbid, viscous, and *flow birefringent*; the bottom liquid is bluish but translucent, nonbirefringent, and of much lower viscosity. The phase separation process is clear-cut within minutes after vigorous shaking, with development of a clear meniscus, denoting a high interfacial tension between the liquids. Therefore, this region is designated as a *double dispersion* (not to be confused with *double emulsion*, a particular type of oil−water emulsion[58]). Region III presents a dense viscous bluish liquid in coexistence with a lower-density clear solution. In region IV, the density of the two phases is reversed. Finally, in region V two clear liquids coexist, with the concentrated viscous solution being the highest density liquid.

B. Electron and Light Microscopic Study. To probe the microstructure of the solution and dispersions observed in Figure 5, both cryo-TEM and light microscopy were carried out. The two techniques in combination allow the visualization of aggregate sizes ranging from 5 to 1000 nm (cryo-TEM) to those larger than 1 μm (light microscopy). The cryo-TEM results for different regions in Figure

(58) Evans, D. F.; Wennerström, H. *The Colloidal Domain*: *Where Physics, Chemistry, Biology and Technology Meet*, 2nd ed.; Wiley-VCH: New York, 1999.

Table 1. Cryo-TEM Observations in the Isotropic Solution and Bluish Dispersion of the STDC−DDAB−Water System at 25 °C

sample	STDC (wt %)	DDAB (wt %)	X_{DDAB}	phase behavior	cryo-TEM observns[a]
A1	4.0	0.9	0.20	L_1	sph mic
A2	3.9	2.0	0.36	region I	domains
A3	3.9	2.1	0.38	region II	domains
B1	8.7		0	L_1	sph mic
B2	8.7	2.2	0.21	L_1	sph mic
B3	8.7	3.3	0.30	region II	sph mic + domains
B4	8.6	3.9	0.32	region III	sph mic + domains

[a] Sph mic refers to spheroidal micelles (ca. 5 nm). Domains refer to large domains (0.2−1 μm) with fine structure.

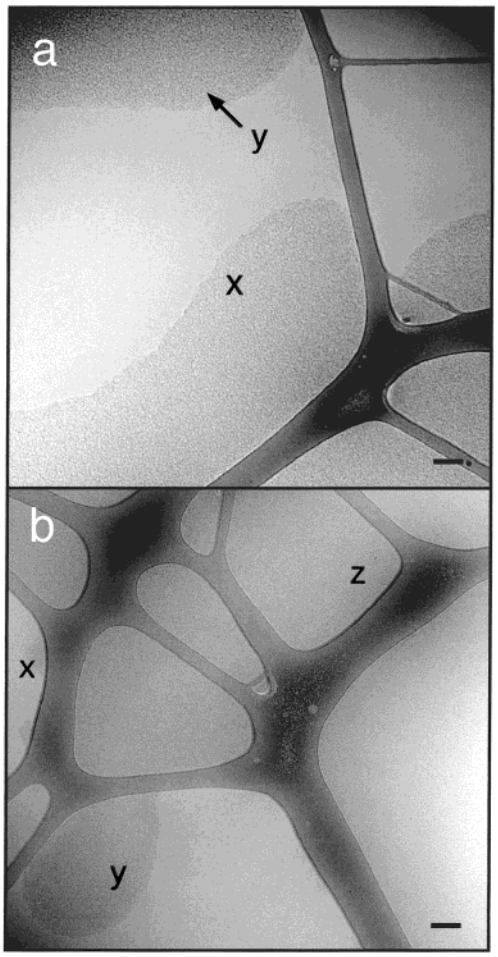

Figure 6. Cryo-TEM imaging of samples in the bluish dispersions of the STDC−DDAB−water system at 25 °C. (a) Bluish dispersion (region I), at 3.9 wt % STDC, 2.2 wt % DDAB (sample A2). Large domains with meshlike, porous structure (x) and sandlike appearance of domain edge (y). (b) Upper phase of double dispersion (region II), at 8.7 wt % STDC, 3.3 wt % DDAB (sample B3). Small (x), medium (y), and large (z) meshlike domains. Bars = 100 nm.

5 are summarized in Table 1. Representative micrographs are shown in Figure 6. The neat bile salt−water solutions (sample B1) show small, spheroidal micellar aggregates of about 5 nm in size. Upon DDAB addition (at X_{DDAB} = 0.2), small micellar aggregates are still present (samples A1 and B2); besides, large domains of irregular size in the order of 100−1000 nm appear in some areas of the film. The bluish region I displays an even higher number of such large structures, as seen in Figure 6a (sample A2). It is possible to observe large domains, 500−1000 nm in size, with a fine dotted structure (*x* in Figure 6a). The interior structure of the domains resembles an array of densely packed micelles. To be noted is the grainy appearance of the domain edge (*y* in Figure 6a). Similar types of structures are depicted in Figure 6b for the upper phase of a sample in region II (sample B3). Small (*x*), medium (*y*), and larger domains filling the grid hole (*z*) can be seen. These micrographs suggest that the observed domains are responsible for the bluish appearance of the dispersions in regions I, II, and III, due the scattering of visible light (Tyndall effect). The domains are clearly not crystallites nor any well-defined surfactant aggregate, such as a vesicle or a large micelle.

To gain further structural insight, light microscopy was also carried out for the bluish dispersions. In Figure 7, a sequence of light micrographs is shown for sample A2. It is clear that the bluish liquid consists of a very fine dispersion of droplets of one liquid in another. The droplets are in Brownian motion and show fast dynamics of coalescence. The droplet size varies from 1 to 100 μm, and it is even possible to see giant droplets containing clusters of smaller ones. From panels a to d in Figure 7, a sequence of events in the time span of 1 min is monitored, during which the area under observation is slightly heated above room temperature by the light beam. In Figure 7a many small droplets are seen in the giant cluster marked as *x*; in Figure 7d, most of small droplets have coalesced into the giant droplet. The process of fusion of a single droplet (marked by an arrow) can be followed in Figure 7.

Figure 8 shows the imaging for the upper (a) and lower (b) bluish liquid phases of sample A3 (*double dispersion* region). The main microscopic difference between the two liquids is that the low-density liquid has larger droplets than the high-density one. The composition of the two liquids is likely to differ. It can be speculated that the upper phase is a dispersion of L in L_1 (low density), while the lower phase is a dispersion of L_1 in L. The flow birefringence of the upper phase is probably due to the anisotropy produced by the shear-induced droplet deformation when the sample is quickly rotated. Upon heating to 40 °C for a few minutes, the two bluish liquids transform into a single white turbid dispersion. Similar observations are made in regions I, II, and III, indicating that the system changes from a *double dispersion* to a typical *strong dispersion* upon increasing temperature.

The combined data from electron and light microscopy show that in the region above the L_1 phase a stable and finely divided dispersion is formed. The dispersion in region I consists then of droplets of the concentrated L_1 phase in a very diluted solution (L). Thus, what is viewed in the cryo-TEM pictures is most certainly the fine structure of the dispersed L_1 domains, which appear to contain small mixed micellar aggregates.

C. NMR Self-Diffusion Study. Self-diffusion measurements were carried out for samples in the L_1 phase and bluish dispersions, to obtain an estimation of aggregate/domain sizes. The self-diffusion coefficients (*D*) for the two surfactants and for water are listed in Tables 2 and 3, respectively. The results at constant 4 wt % STDC and increasing X_{DDAB} are shown in Figure 9a. In the L_1 phase both surfactants have similar *D* values. *D* decreases from 9.1×10^{-11} m^2 s^{-1} for the neat STDC solution to 5.1×10^{-11} m^2 s^{-1} for a solution at $X_{DDAB} = 0.20$, showing that the micellar growth is not pronounced. In effect, the aggregate hydrodynamic radius R_H, estimated from the Stokes−Einstein equation, uncorrected for intermicellar obstruction effect, increases from 21 Å for the neat bile salt micelle to 44 Å for the mixed aggregate at X_{DDAB} = 0.20 (Figure 9b).

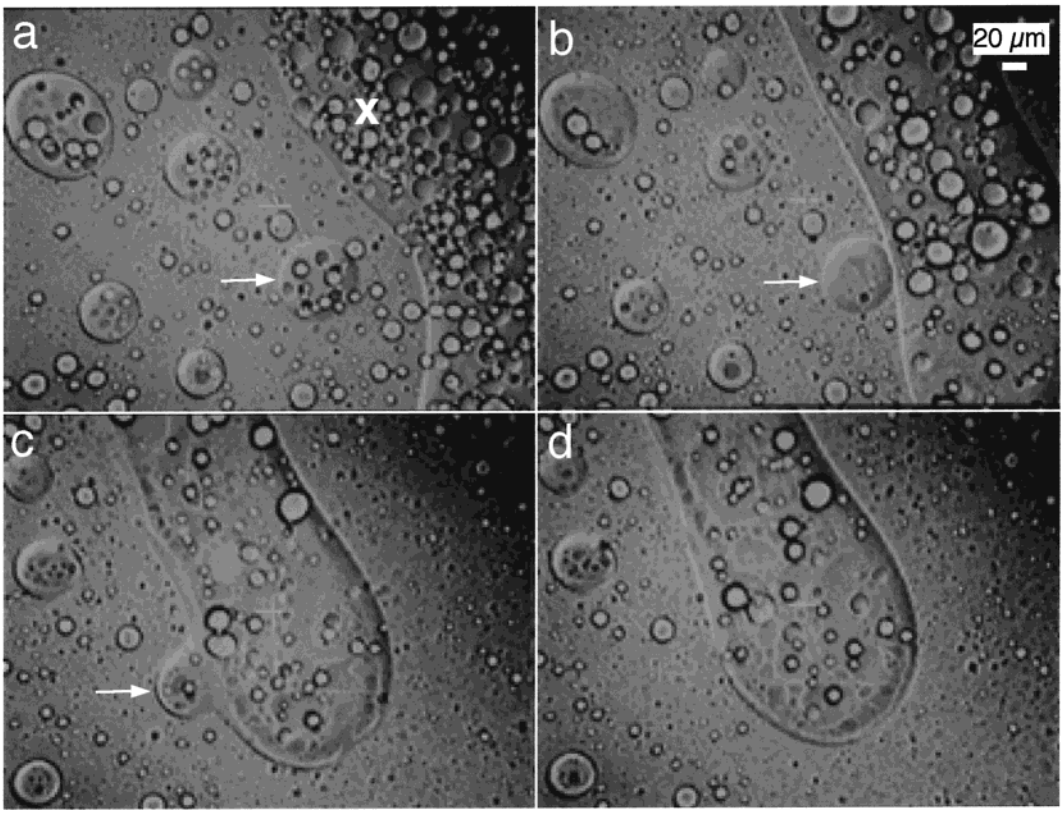

Figure 7. Imaging of a bluish dispersion, at 3.9 wt % STDC, 2.0 wt %, in the light microscope. From (a) to (d), there is a time delay of ca. 60 s. The arrow points to the coalescence process of a small droplet. Note also that the small droplets clustered inside the giant droplet (marked with *x*) eventually coalesce. Since the dispersion is stable at room temperature, this effect appears to result from the slight increase in temperature provided by the light beam.

In the bluish region (region I), however, a different trend is observed. The DDAB diffusion is consistently slower than the STDC one, by a 1.5−3-fold factor. As X_{DDAB} increases, the discrepancy between the two D values increases. It was also possible to measure the surfactant diffusion in the two bluish dispersions of region II. The coefficients for the upper phase are considerably smaller than those for the lower phase, as expected from previous viscosity observations. R_H values obtained from the DDAB diffusion (Figure 9b) yield 17 and 570 nm for the lower and the upper phase, respectively. Further self-diffusion measurements made for more concentrated samples in the L_1 solution and bluish dispersion regions are listed in Table 2. The D values obtained for the equimolar sample at 34.6 wt % STDC/30.5 wt % DDAB, roughly in the range of 1×10^{-12} m^2 s^{-1} for both surfactants, suggest also the presence of small mixed aggregates. The estimated radii (R_H) in Table 1 allow only qualitative discussions, since at these surfactant concentrations interaggregate obstruction effects have an important contribution to the measured D (consequently, the radii in Table 2 are overestimated). For other L_1 samples in Table 2, with $X_{DDAB} = 0.2-0.35$, both surfactants show similar D values ($6-7 \times 10^{-13}$ m^2 s^{-1}), meaning slightly slower diffusion than in the equimolar solution.

Water self-diffusion provides further information on the aggregation phenomena. The reduced self-diffusion coefficients, D/D_o in Table 3, give a qualitative indication of the obstructing volume for free water diffusion. Only Gaussian (*free*) diffusion is observed for both solutions and dispersions, i.e., only a single diffusion coefficient is obtained, and no restricted diffusion occurs. At 4 wt % STDC and $X_{DDAB} = 0-0.36$, the decrease in D/D_o is not very significant. However, at $X_{DDAB} = 0.38$ (region III), the upper dispersion shows a pronounced decrease in D/D_o, while the lower dispersion shows a value close to that of neat water. These results are consistent with the much higher viscosity of the upper dispersion. On the other hand, it is interesting to note that in the lower bluish dispersion, D/D_o is comparable to that for the neat bile salt micellar solution. D/D_o for the concentrated L_1 varies between 0.2 and 0.5, consistent with high obstructing volume (high viscosity) for these solutions.

A global analysis of the self-diffusion study allows some conclusions with respect to phase microstructure. The DDAB self-diffusion in the bluish dispersion is similar to that in the concentrated L_1 phase, but slightly faster due to the dilution effect (lower obstructing volume).This fact supports the view that the bluish liquids consists of a fine dispersion of L_1 in a diluted solution. The discrepancy found between the STDC and DDAB coefficients in the bluish dispersions (not seen in the concentrated L_1) can be reasonably explained. The faster STDC diffusion results most probably from the averaging of the diffusion of "pure" STDC micelles in the diluted solution (fast diffusion) and the mixed aggregates in the concentrated L_1 domains (slow diffusion). This averaging requires a fast exchange of STDC monomer between the two aggregates. Some evidence for this interpretation comes from cryo-TEM observations, where small micelles appear to coexist with the large domains (data not shown here). In turn, the water diffusion for the double dispersion allows some speculation on its structure. The microscopy results indicate a droplet structure for both dispersions. The water and surfactant diffusion are consistent with the upper birefringent dispersion being a highly concentrated dispersion of aggregated L_1 domains (droplets) in the L phase or a dilute dispersion of L droplets in L_1. The lower bluish

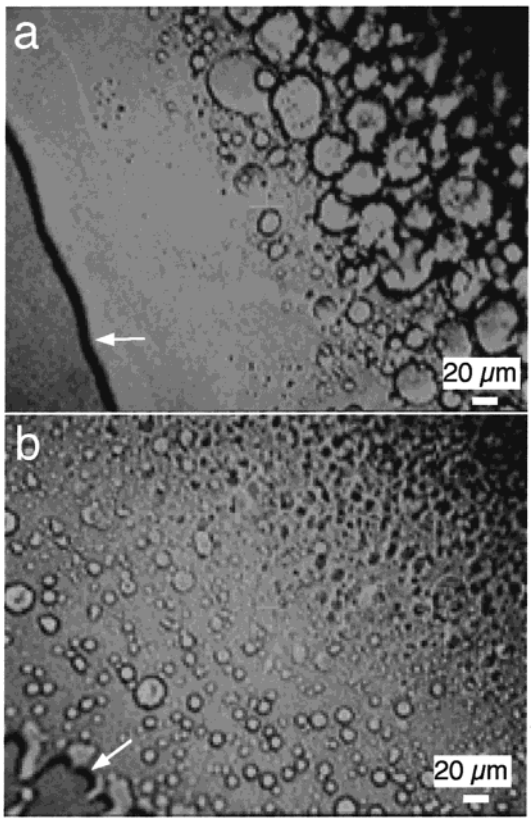

Figure 8. Light microscopy imaging of a sample in the *double dispersion* region, at 3.9 wt % STDC, 2.2 wt %: (a) upper phase; (b) lower phase. The arrows indicate the air−liquid boundary for the sample in the glass slide.

Table 2. Surfactant Self-Diffusion Coefficients Obtained from PFG NMR in the Solutions and Bluish Dispersions of the STDC−DDAB−Water System at 25 °C

STDC (wt %)	DDAB (wt %)	X_{DDAB}	phase behavior	D_{STDC} (10^{-12} m^2 s^{-1})	D_{DDAB} (10^{-12} m^2 s^{-1})	R_H[a] (nm)
4.0	0	0	L_1	91		1.7
4.0	0.2	0.06	L_1	85	76	2.5
4.0	0.9	0.20	L_1	51	44	4.4
3.9	2.0	0.36	region I	8.7	2.9	321
3.9	2.2	0.38	region II[b]	1.5	0.34	572
3.9	2.2	0.38	region II[c]	24	11	17.2
7.5	3.1	0.32	region I	46	18	11.0
8.6	4.5	0.30	region I	0.79	0.85	304
25.3	6.0	0.21	L_1	0.65	0.47	413
28.7	10.9	0.30	L_1	0.61	0.61	321
30.0	12.9	0.33	L_1	0.60	0.65	299
34.6	30.5	0.49	L_1	0.78	1.1	250
37.06	28.1	0.46	L_1	0.76	0.90	258

[a] Values calculated from D_{DDAB}. [b] Region II (upper phase). [c] Region II (lower phase).

dispersion must then be essentially a diluted dispersion of L_1 droplets in L. The reasons behind their equilibrium phase separation remain puzzling and require further investigations.

4. Summary and Final Remarks

The STDC−DDAB−water system illustrates a catanionic system in which several uncommon phase behavior features are observed. At room temperature, two single-phase regions are observed in the bile salt-rich area: a wide isotropic solution, extending to equimolarity, and a hexagonal liquid-crystalline phase, which incorporates small amounts of DDAB. Self-diffusion and cryo-

Table 3. Water Self-Diffusion Coefficients in the Solution and Dispersions of the STDC−DDAB−Water System at 25 °C

STDC (wt %)	DDAB (wt %)	X_{DDAB}	phase behavior	D_{HDO} (10^{-9} m^2 s^{-1})	D/D_o[a]
4.0	0	0	L_1	1.81	0.951
4.0	0.9	0.20	L_1	1.77	0.932
3.9	2.0	0.36	region I	1.69	0.891
3.9	2.2	0.38	region I[b]	1.19	0.624
3.9	2.2	0.38	region II[c]	1.86	0.980
25.3	6.0	0.21	L_1	1.03	0.542
28.7	10.9	0.30	L_1	0.808	0.425
30.0	12.9	0.33	L_1	0.702	0.369
37.1	28.1	0.46	L_1	0.316	0.166

[a] Ratio between the observed diffusion coefficient, D, and that for neat water (HDO), $D_o = 1.90 \times 10^{-9}$ m^2 s^{-1}. [b] Region I (upper phase). [c] Region II (lower phase).

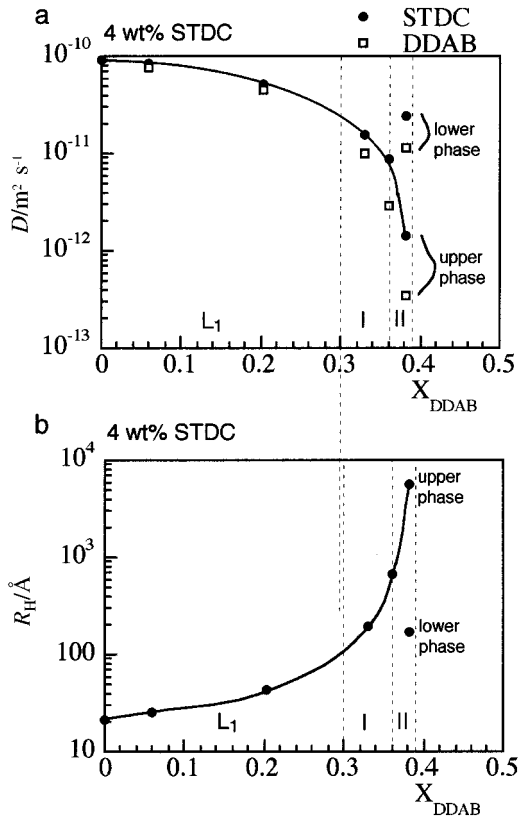

Figure 9. Self-diffusion measurements in the dilute region of the STDC−DDAB−water system, at 25 °C: (a) surfactant self-diffusion; (b) hydrodynamic radius calculated from the self-diffusion coefficient values for DDAB. The lines are guides for the eye.

TEM data show that the mixed micellar aggregates in the L_1 region do not grow significantly, neither as a function of DDAB nor of total surfactant concentration. The hexagonal lc phase has been tentatively assigned to a reverse type structure.[17,18] The destabilization of a reverse hexagonal phase by addition of DDAB then appears somewhat curious, since DDAB in principle would comfortably pack in a structure of negative curvature, as seen for instance in the DDAB−AOT system.[43] The easy perturbation of the lc phase by the flexible chain amphiphile thus suggests a highly nonconventional reverse type structure. From the phase diagram, it follows that the isotropic solution phase is favored upon DDAB addition. So one can speculate on the diverse structure of the aggregates in the lc phase and in the L_1 phase, despite the "proximity" in bulk composition. No cubic liquid-crystalline phase is formed around equimolar composi-

tions, in contrast to several bile salt−surfactant systems[20,28,34] and catanionic systems in general.[37,43,59]

The region between the L_1 phase and the equimolar line is a two-phase region composed of L_1 and a very dilute solution (almost pure water), where the macroscopic separation between the phases takes some peculiar aspects upon DDAB addition. Equimolarity is dominated by "true" coacervation, i.e., complete macroscopic phase separation of the two solutions. The intermediate region of the phase diagram is dominated by a very fine bluish dispersion of L_1 in the diluted phase. While the bluish dispersion is in equilibrium with the diluted phase at higher X_{DDAB} (region III), at lower X_{DAAB} it occurs on its own (region I) or separates into a concentrated and a dilute dispersion (*double dispersion* region). As DDAB is further added, the concentrated L_1 domains gradually separate from the almost pure water phase, and this is eventually attained at around equimolarity.

For most common catanionic surfactant systems, the concentrated phase is either a precipitate or a liquid-crystalline phase.[42] This is not the case for the STDC−DDAB mixture, where the mixed aggregates at equimolarity retain the micellar structure. Moreover, vesicle formation, often detected in catanionic mixtures, is absent from the diluted bile salt-rich area of the system. This absence is to some extent surprising since DDAB is a bilayer-forming surfactant and the bile salt has a versatile amphiphilic structure. The current system illustrates the effectiveness of both STDC and DDAB as dispersants (or emulsifiers). The bile salt is the highly efficient fat emulsifier in the body, its biological importance thereof derived.[3,7] DDAB is known to form extensive regions of microemulsions with a number of oils.[60] The two amphiphiles in combination show strong synergistic properties. These observations are probably generalized to other types of bile salt−double-chained surfactant mixtures, but the electrostatic effects in catanionic systems are likely to enhance the dispersive power.

Acknowledgment. Camillo La Mesa is kindly acknowledged for many valuable discussions. The Swedish Research Council for Engineering Sciences (TFR) and PRAXIS XXI, Portugal (project 2/2.1/QUI/411/94), are gratefully acknowledged for financial support. H.E. gratefully acknowledges STINT (The Swedish Foundation for International Cooperation in Research and Higher Education) for a Postdoctoral Scholarship in the Department of Chemical Engineeering, University of Delaware.

LA0002278

(59) Edlund, H.; Sadaghiani, A.; Khan, A. *Langmuir* **1997**, *13*, 4953.

(60) Warr, G. G.; Sen, R.; Evans, D. F.; Trend, J. E. *J. Phys. Chem.* **1988**, *92*, 774.